EPJ Web of Conferences **288**, 07009 (2023) https://doi.org/10.1051/epjconf/202328807009
*ANIMMA 2023*

# Neutron imaging with Micromegas detectors with optical readout

*A.* Cools[1,*], *S.* Aune[1], *F.M.* Brunbauer[2], *T.* Benoit[1], *A.* Corsi[1], *E.* Ferrer-Ribas[1], *F.J.* Iguaz[3], *C.* Mazoin[4], *E.* Oliveri[2], *T.* Papaevangelou[1], *E.C.* Pollacco[1], *M.* Potignon[4], *L.* Ropelewski[2], *A.* Sari[5]

[1]DRT, IRFU, CEA, Université Paris-Saclay, F-91191 Gif-sur-Yvette, France
[2]European Organization for Nuclear Research (CERN), 1211 Geneva 23, Switzerland
[3]SOLEIL Synchrotron, L'Orme des Merisiers, Départementale 128, 91190 Saint-Aubin, France
[4]DG, SPRE, CEA, Université Paris-Saclay, F-91191 Gif-sur-Yvette, France
[5]DRT, LIST, CEA, Université Paris-Saclay, F-91191 Gif-sur-Yvette, France
(*) antoine.cools@cea.fr

**Abstract.** **Optical readout of Micromegas gaseous detectors has been achieved by implementing a Micromegas detector on a glass substrate with a glass anode and a CMOS camera. Efficient X-ray radiography has been demonstrated due to the integrated imaging approach inherent to optical readout. High granularity values have been reached for low-energy X-rays from radioactive sources and X-ray generators taking advantage of image sensors with several megapixel resolution. Detector characterization under X-ray radiography opens the way to different applications from beta imaging to neutron radiography. Here we will focus on one application: neutron imaging for non-destructive examination of highly gamma-ray emitting objects. This article reports the characterization of the detectors when exposed to a low activity neutron source. The response of the detector to thermal neutrons has been studied with different field configurations and gap thicknesses.**

## I Introduction

The optical readout Micromegas detector is a brand new imaging device taking advantage of the CMOS sensor technology of high granularity and sensitivity. A Micromegas detector [1] of high intrinsic gain and spatial resolution has been implemented on a transparent anode. When operated with a mixture of Carbon tetrafluoride ($CF_4$) and Argon, visible light is produced by scintillation when ionization occurs. This detector has shown high spatial resolution under X-ray irradiation and was able to detect very low activity $\beta$-ray emitting samples [2, 3].

Coupling MicroPattern Gaseous Detectors (MPGDs) with a metallic cathode coated with $^{10}B_4C$, a neutron to charge converter, leads to a thermal neutron detection device, with efficiency of few percent and high gamma suppression capability [4]. Such a neutron converter has been used with an optical readout Micromegas detector aiming at performing real-time imaging of neutron sources with 100 µm spatial resolution.

Neutron radiography allows to characterize reactor materials like radioactive waste or nuclear fuel in a high $\gamma$-flux environment. First images of neutron events from a weak neutron source were acquired and reported in [2]. The Micromegas cathode (an aluminum plate) is coated with 1.5 µm of $^{10}B_4C$ which converts the thermal neutrons into $^7$Li and $\alpha$ of 0.8 MeV and 1.4 MeV respectively, having a range in the gas of few mm. The present article describes the analysis of the tracks giving information about the diffusion in the gas and the neutron incident position on the cathode. Different field configurations were tested with a 10.5 mm conversion gap. A new setup with a 250 µm drift gap was tested in order to reduce the track range and to perform double stage amplification.

## II Neutron radiography

The main goal of the glass Micromegas detector is to reach high spatial resolution for real-time neutron imaging. The capacity of the camera to integrate the light makes the detection of the neutron impact position feasible with very few data processing which allows to display the neutron image in real-time. However, the spatial resolution of the device is strongly affected by the diffusion and the particle range inside the gas. In the first parts of this section, the analysis of the $^7$Li and $\alpha$ tracks from neutron events is described. In a second step, the reconstruction of the neutron impact position with two different drift gap thicknesses is explained and illustrated.

### II.A Experimental setup

This test was performed at the CERN Gas Detector Development (GDD) laboratory with an Americium–Beryllium source, emitting 1–14 MeV neutrons with a detection rate of 4 Hz in average. The main characteristics of the glass Micromegas detector, of the chosen gas mixture and the CMOS camera are fully described in previous work [2]. The drift gap is of 10.5 mm in order to contain the full

*e-mail: antoine.cools@cea.fr

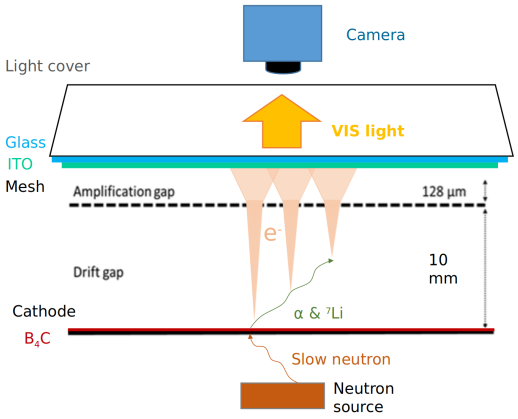


Figure 1: Sketch of the glass Micromegas detector setup for neutron radiography. Neutrons are interacting in the $^{10}B_4C$ layer producing $^7$Li and $\alpha$ particles emitted back-to-back. The gas is ionized along the $^7$Li or $\alpha$ tracks and the produced electrons drift towards the amplification gap. In the amplification gap, they are multiplied, producing also visible light captured by the camera.

tracks. The amplification gap is 128 µm and the applied voltage 570 V (Figure 1). At this voltage value, discharges occur rarely and bring almost no dead-time of the detector while the ITO layer remains undamaged. Due to the low rate of the source, 5 s exposure time images were acquired in order to collect several tracks in one frame, while avoiding overlap of tracks. Background images of the same integration time were recorded without any applied voltage or neutron source. Matrices of the average and standard deviation of every pixel of dark images are then computed for background suppression.

### II.B Tracks analysis and results

The analysis of the images is done in Python and aims to localize the tracks in a first step. The background noise coming from the dark current and the readout noise of the camera constitutes the pedestal of an image. The pixels intensity (0 to 65536) of dark images correspond to 0 photons and varies from one pixel to another as shown in Figure 2. These histograms represent the mean ($\mu_i$) and standard deviation ($\sigma_i$) of every pixel $i$ intensity. First, the $\mu_i$ are suppressed from the neutron images and a threshold of $3\sigma_i$ is applied on every pixel in order to reject most of the background noise. To increase the signal to noise ratio, the new neutron image is rescaled to a $1024 \times 1024$ pixels frame by applying a $2 \times 2$ binning.

The clustering algorithm employed for track identification is the so-called Density-Based Spatial Clustering of Applications with Noise (DBSCAN)[5]. This algorithm measures the distance between points and generates three categories of points :

- A core point is localized in an area of high density of points and is generally situated in the center of a cluster.
- A reachable point is at a distance $\epsilon$ of a core point and constitutes the cluster surrounding.

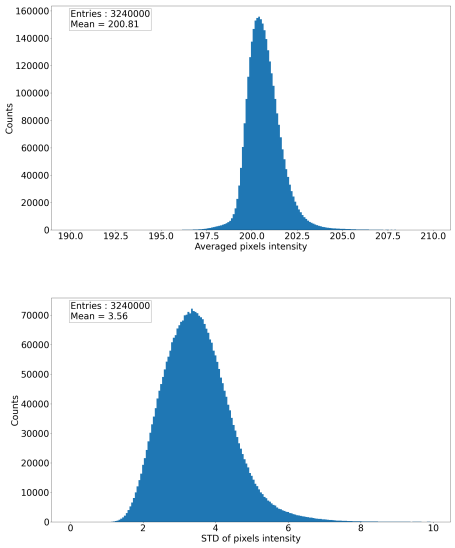


Figure 2: Mean (top) and standard deviation (bottom) histograms of pixels intensity from dark images.

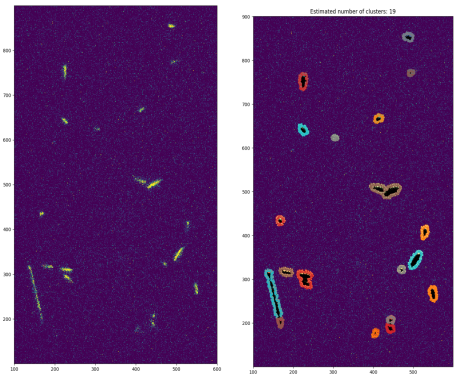

Figure 3: Neutron image before (left) and after (right) clusters identification by the DBSCAN algorithm.

- A noise point is not reachable by any other points within the distance $\epsilon$.

Only the clusters containing a minimum number of points *MinPts* are kept. Hence, this algorithm requires only the matrix of pixel intensities as an input and $\epsilon$ and *MinPts* as parameters. No optimization of the $\epsilon$ and *MinPts* parameters has been done yet. However, most of the tracks are being well identified and separated (Figure 3).

From the clustering algorithm, we access the coordinates of all the tracks. It is then possible to measure the width of the tracks by integration of the 2D track image over the track length. The Gaussian fit of the integrated intensity directly gives a $\sigma$ value corresponding to the diffusion in the gas. The transverse diffusion is given by the equation $\sigma_D = \sqrt{2Dt}$ where $D$ is the diffusion coefficient, function of the electric field ($E$), and $t$ is the drift time.

According to Magboltz [6] simulations, the smallest transversal diffusion coefficient value corresponds to E $\approx$ 700 V/cm for a gas mixture with 80% of Ar and 20% of $CF_4$ (Figure 4). First measurements were taken with the same gas mixture at three different drift fields: 50 V/cm,

800 V/cm and 2000 V/cm. The measured diffusion was around 130 µm for a 800 V/cm drift field whereas the $\sigma$ value reached higher values for the other two drift field configurations (Figure 4). The simulated diffusion evolution agrees within $2\sigma$ with the extracted points from measured track widths meaning that the broadening of the tracks is mainly due to diffusion.

However, the tendency of the measured data of having lower values than the simulated ones could be justified by the following: in the simulation, we consider that every electron is emitted at the cathode level and diffuses all along the drift gap. In reality, free electrons are generated all along the track and a majority is produced at the end of the track, at a distance from the cathode. By drifting a shorter distance, their diffusion is smaller, so the extracted values for the coefficient are systematically lower. In fact, the diffusion increases with the depth $x$ as $\sqrt{x}$ which brings a difference of few tens of % between the diffusion at the cathode level and at the end of the track. Another consideration that may have an effect is the absence of monitoring of the temperature and pressure conditions that strongly affect the diffusion.

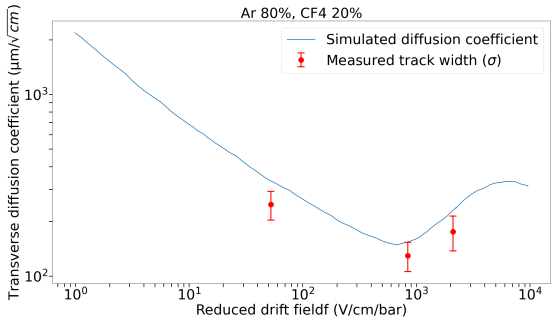


Figure 4: Simulated transverse diffusion in 80% of Ar and 20% of $CF_4$. Average track width ($\sigma$) from measurements.

## II.C Neutron position reconstruction

It is possible to overcome the incertitude on the neutron position brought by the track length by fitting the Bragg peak of a track. In fact, the $^7$Li and $\alpha$ particles deposit more energy in the gas at the end of their path. This means that the neutron position of interaction with the cathode is localized at the lowest point of the Bragg curve. 60 000 events were analyzed and associated to a position of interaction by fitting the Bragg peak with a linear distribution and represented on an histogram (Figure 5). A copper tape band was glued on the boron side of the cathode so that $^7$Li and $\alpha$ particles are absorbed in one side only of the detector. The spatial resolution is then calculated by fitting the edge with a step function $f$ described in (1) where $\mu$ is the edge position and A is the maximum amplitude. A spatial resolution of $\sigma$ = 1420 (±124) µm was obtained.

$$f(x) = \frac{A(1 + erf(p))}{2} \qquad p = \frac{(x - \mu)}{\sqrt{2}\sigma} \qquad (1)$$

The image on Figure 6 represents the light intensity profile obtained by integrating the light coming from the tracks. Here the precision on the neutron position measurement is affected by the particles range and should lead to a larger spatial resolution. However, the spatial resolution obtained from the reconstruction method and from the light integration method (1198 (±263) µm) are of the same order. This means that the fit of the Bragg peak fails in some cases. Further study on the simulation of the $^7$Li and $\alpha$ tracks and on the reconstruction algorithm are needed.

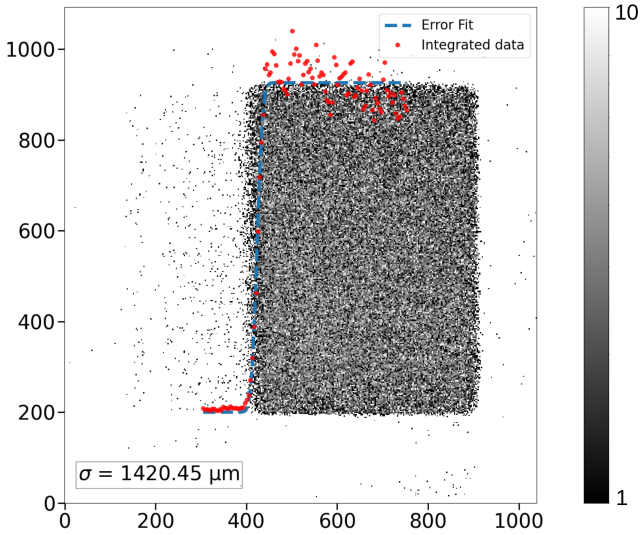


Figure 5: Neutron position histogram for a 10.5 mm drift gap.

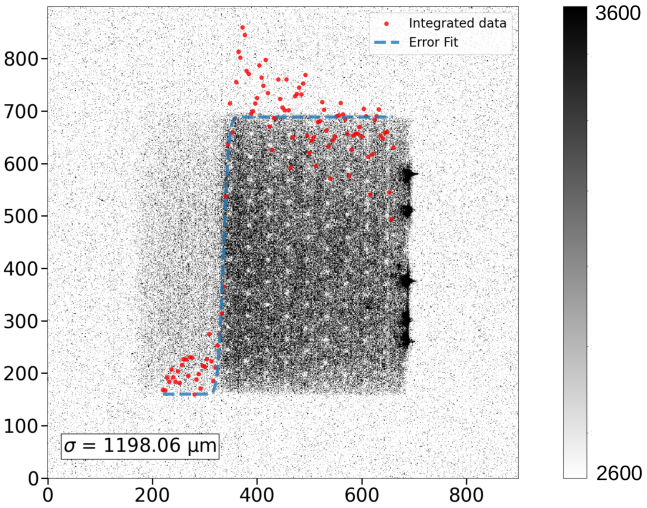


Figure 6: Neutron light intensity profile for a 10.5 mm drift gap.

A new configuration with a 250 µm drift gap was tested in order to reduce significantly the particles range in the gas. Then the error on the position computation brought by the track length is expected to decrease. As a consequence, less charges are produced in the gas, decreasing the signal intensity. By generating an electric field of 20 kV/cm in the drift gap, a double stage amplification leads to a higher gain and compensate the lack of primary electrons. More-

over, the gain increases with the avalanche length which means that primary electrons that are produced close to the cathode are amplified further. This mechanism enhances the signal at the neutron impact position. In this configuration, clusters with a Gaussian shape were recorded instead of track shapes. Hence, implementing a $2D$ Gaussian fit of the clusters allows to reconstruct the neutron position with a better precision (Figure 7).

It is not possible to use a copper tape in this setup since the copper thickness is not negligible and would affect the electric field in such a small gap. However, boron evaporation on the cathode with a mask with patterns will be realized in the future for spatial resolution measurement without affecting the electric field. A boron band was placed outside of the detector on one side with the ambition of visualizing an edge. Because of the large angle neutrons, an important number of events were detected on the side where the boron was put, making the edge image very blurred. On the right side of the histogram, the density of hits is not homogeneous along the y-axis. Mechanical constraints on the cathode brought defaults on its planarity of few tens of µm which caused a non uniform gain in the drift gap during double stage amplification.

However, the 500 µm diameter pillars are well resolved in the right side of this histogram. The assessment of the pillars position is an indication that a spatial resolution of a few hundred µm can be achieved. The low spreading of the charges in this configuration will allow us to perform real time neutron radiography by simply integrating the light intensity over time for high flux sources.

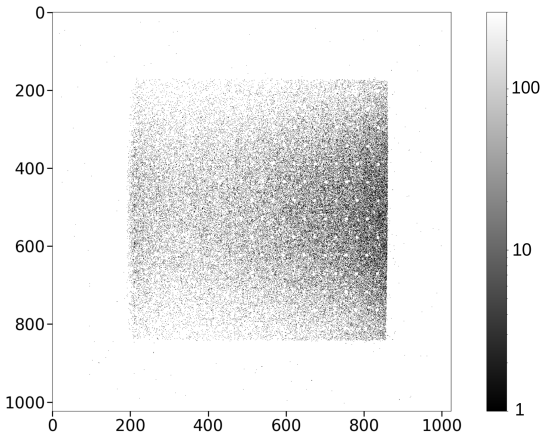


Figure 7: Neutron position histogram for a 250 µm drift gap with double stage amplification.

## III Conclusion

Neutron events were detected with a glass Micromegas detector and studied under different field configurations. The diffusion from the ionization of $^7$Li and $\alpha$ particles was measured and compared to computed diffusion from simulation. Two methods were explored in order to increase the spatial resolution. The first one consisted in the reconstruction of the neutron impact position on the cathode. A spatial resolution better than 1500 µm was achieved. In a second step, double stage amplification was performed with a 250 µm drift gap in order to reduce the particle range and to emphasize the neutron position. The spatial resolution was not measured in this configuration because of the lack of statistics and the non-parallelism of the neutrons. In the near future, a neutron beam test will be conducted at a neutron facility with a high flux source of parallel thermal neutrons for precise estimation of the spatial resolution with different field configurations and gap thicknesses.

## References

[1] Y. Giomataris. “Development and prospects of the new gaseous detector “Micromegas””. In: *Nuclear Instruments and Methods in Physics Research Section A: Accelerators, Spectrometers, Detectors and Associated Equipment* 419.2 (1998), pp. 239–250. ISSN: 0168-9002. DOI: https : / / doi . org / 10 . 1016 / S0168 - 9002(98 ) 00865 - 1. URL: https : / / www . sciencedirect . com / science / article / pii / S0168900298008651.

[2] A. Cools et al. “Neutron and beta imaging with Micromegas detectors with optical readout”. In: *Nuclear Instruments and Methods in Physics Research Section A:Accelerators, Spectrometers, Detectors and Associated Equipment* 1048 (2023), p. 167910. ISSN: 0168-9002. DOI: https://doi.org/10.1016/j.nima.2022.167910. URL: https://www.sciencedirect.com/science/article/pii/S0168900222012025.

[3] A. Cools et al. *X-ray imaging with Micromegas detectors with optical readout*. 2023. arXiv: 2303 . 17444 [physics.ins-det].

[4] T. Papaevangelou et al. “ESS nBLM: Beam Loss Monitors based on Fast Neutron Detection”. In: *Proc. 61st ICFA Advanced Beam Dynamics Workshop (HB’18), Daejeon, Korea, 17-22 June 2018* (Daejeon, Korea). ICFA Advanced Beam Dynamics Workshop 61. https://doi.org/10.18429/JACoW-HB2018-THA1WE04. Geneva, Switzerland: JACoW Publishing, July 2018, pp. 404–409. ISBN: 978-3-95450-202-8. DOI: doi : 10 . 18429 / JACoW - HB2018 - THA1WE04. URL: http : / / jacow . org / hb2018/papers/tha1we04.pdf.

[5] Martin Ester et al. “A Density-Based Algorithm for Discovering Clusters in Large Spatial Databases with Noise”. In: *Proceedings of the Second International Conference on Knowledge Discovery and Data Mining*. KDD’96. Portland, Oregon: AAAI Press, 1996, pp. 226–231.

[6] S. F. Biagi. “Monte Carlo simulation of electron drift and diffusion in counting gases under the influence of electric and magnetic fields”. In: *Nucl. Instrum. Meth. A* 421.1-2 (1999), pp. 234–240. DOI: 10.1016/S0168-9002(98)01233-9.